Research Square

Preprints are preliminary reports that have not undergone peer review.
They should not be considered conclusive, used to inform clinical practice,
or referenced by the media as validated information.

A hybrid direct FE2 method for composite materials with interface damage using failure and strain gradient indices to identify critical regions

Ju-Won Jin
Seoul National University of Science and Technology
Hyun-Gyu Kim
khg@seoultech.ac.kr

Seoul National University of Science and Technology

Research Article

Keywords: Multiscale analysis, Direct FE² method, Asymptotic homogenization, Tsai-Wu failure index, Stress gradient index, Cohesive zone model

Posted Date: November 23rd, 2026

DOI: https://doi.org/10.21203/rs.3.rs-11647770/v1

License: This work is licensed under a Creative Commons Attribution 4.0 International License.
Read Full License

Additional Declarations: No competing interests reported.

A hybrid direct FE^2 method for composite materials with interface damage using failure and strain gradient indices to identify critical regions

Ju-Won Jin[a] · Hyun-Gyu Kim[a,*]

[a] Department of Mechanical Engineering, Seoul National University of Science and Technology, 232 Gongneung-ro, Nowon-gu, Seoul, 01811, South Korea

Keywords: Multiscale analysis · Direct FE² method · Asymptotic homogenization · Tsai-Wu failure index · Stress gradient index · Cohesive zone model

Abstract

This paper proposes a hybrid direct FE² method that combines the computational efficiency of the homogenization method with the accuracy of the direct FE² method to efficiently simulate the interface failure in composite materials. A critical failure index based on the Tsai-Wu failure criterion is determined by comparing macroscopic homogenization and direct FE² analyses of an RVE subjected to a range of training loads. The composite structure is first analyzed using a homogenized finite element model, and the critical failure index is then used to identify regions susceptible to interfacial failure. These regions are subsequently replaced by direct FE² domains, in which cohesive elements are placed along the fiber–matrix interfaces. The direct FE^2 method is also applied to regions with high stress gradients, where the homogenized macroscopic elements lose accuracy. Numerical results show that the proposed hybrid direct FE^2 method substantially reduces computational cost compared with the full direct FE² method while preserving accuracy in simulating interface failure in composite materials.

* Corresponding author

E-mail address: khg@seoultech.ac.kr (H.-G. Kim).

1. Introduction

Composite materials have been extensively used in a wide range of engineering fields, including the energy, automotive, and aerospace industries, owing to their high strength-to-weight ratio and excellent durability. However, accurately predicting their macroscopic behavior requires substantial computational resources because of their complex microstructures. Representative approaches developed to reduce this computational burden include homogenization methods [1,2] and multiscale finite element methods [3,4]. Homogenization methods substantially improve efficiency by extracting the effective properties of a representative volume element (RVE) under periodic boundary conditions and applying them to the macroscopic model. While this approach predicts the macroscopic behavior of composites at low computational cost, it is inherently limited in capturing the nonlinear behavior within the RVE, such as strain localization, local damage, and plastic deformation.

As a multiscale analysis framework, the FE^2 method couples the two scales iteratively, solving an RVE problem at each macroscopic integration point until convergence is achieved. FE^2-based models have been widely applied to a broad range of problems in composite mechanics. The conventional FE^2 procedure, however, is difficult to implement in practical applications, and becomes computationally expensive for nonlinear problems because the microscale solution is nested within the macroscopic process in a staggered solution scheme. The direct FE^2 method [5] has been proposed to alleviate these difficulties by linking macro-scale FEs to micro-scale FEs into a single unified finite element model solved with a monolithic solution scheme. The direct FE^2 method accurately captures local nonlinearity and path dependence by placing an RVE at each integration point of the macroscopic elements and connecting the two scales through multi-point constraints (MPCs). In the direct FE^2 method, both scales are solved in a single analysis, eliminating the iterative coupling required in conventional FE^2 methods. The micro-scale finite element models, however, still require a large number of degrees of freedom to properly represent the mechanical behavior of RVEs, which makes the method impractical for large-scale problems.

A homogenized model captures the global behavior of composite structures efficiently, whereas detailed models with fully resolved RVEs provide more accurate predictions in local regions undergoing severe deformation. Consequently, the computational cost of multiscale analyses can be significantly reduced by combining a homogenized global model with refined models in the critical local regions [6]. To identify such regions requiring detailed analysis, earlier studies monitored whether the macroscopic stress state reaches a predefined threshold [7]. More recently, a hybrid method based on the strain gradient has been developed to simulate strain localization in multiscale structures, in which fully resolved finite element models are used directly in the local regions to capture the details of strain localization [8]. Adaptive multiscale frameworks have also been proposed to capture macroscopic failure coupled with microscopic interfacial delamination [9,10]. Despite these advancements, existing adaptive hybrid techniques typically rely on either a simple error indicator or a single criterion to determine the regions requiring detailed analysis. Consequently, when complex multiaxial loading is applied to composite structures or when damage and abrupt stress distribution occur simultaneously, such criteria may fail to capture local degradation, so that the refined models are placed where

they are unnecessary and omitted where they are needed. A more robust and comprehensive switching strategy is therefore required to reliably identify regions that demand microscopic resolution.

Accordingly, this study proposes a damage-based hybrid technique that identifies critical regions by combining a Tsai-Wu failure index with a stress gradient index and applies the direct FE² method only within these regions. The strength parameters of the failure index are determined by analyzing an RVE under a set of training loads. These regions identified by the failure index are then replaced by fully-resolved RVEs with cohesive elements along the fiber-matrix interfaces. The stress gradient index is used to identify additional regions requiring direct FE² analysis, thereby further reducing the error in the homogenized elements, which cannot properly represent stress variations among RVEs within a macro-element. Since the remainder of the domain is represented by homogenized elements, the proposed hybrid method substantially reduces the computational cost. The remainder of this paper is organized as follows. Section 2 and Section 3 describe the mathematical formulation and numerical implementation of the direct FE² method and the asymptotic homogenization method. Section 4 presents the proposed hybrid direct FE² method, in which elements are replaced automatically on the basis of the failure index (FI) and the stress gradient index (SGI). In Section 5, the cohesive zone model (CZM) is introduced to describe interfacial failure, and the proposed algorithm is applied to three numerical examples, a cantilever beam, an S-shaped beam, and a mode I edge-cracked specimen, to quantify the efficiency of the proposed method over the conventional direct FE² method and the accuracy relative to the homogenized model. Finally, Section 6 summarizes the main findings and concludes the paper.

2. Direct FE² method

The direct FE² method is a concurrent multiscale technique in which an RVE is placed at each integration point of the macroscopic mesh, so that information is exchanged between the scales without an explicit homogenization step. This study adopts a direct FE² framework based on the Hill-Mandel homogenization principle [11]. Applying the principle of virtual work under the prescribed macroscopic loading yields the coupled macro– and micro-governing equations:

$$\delta\tilde{\boldsymbol{u}}^{\mathrm{T}}\tilde{\boldsymbol{K}}\tilde{\boldsymbol{u}} = \delta\tilde{\boldsymbol{u}}^{\mathrm{T}}\tilde{\boldsymbol{F}} \tag{1}$$

$$\delta\boldsymbol{u}^{\mathrm{T}}\boldsymbol{K}\boldsymbol{u} = \delta\boldsymbol{u}^{\mathrm{T}}\boldsymbol{F} \tag{2}$$

where $\boldsymbol{u}$ indicates the macroscopic displacement vector, and $\tilde{\boldsymbol{u}}$ the microscopic displacement vector. The Hill–Mandel condition requires that the volume average of the microscale fields over the RVE equal the corresponding macroscale physical quantities. Eqs. (1) and (2) then give

$$\delta\tilde{\boldsymbol{u}}^{\mathrm{T}}\tilde{\boldsymbol{K}}^{*}\tilde{\boldsymbol{u}} = \delta\boldsymbol{u}^{\mathrm{T}}\boldsymbol{F} \tag{3}$$

Since micro-finite elements have a smaller physical volume compared to macro-elements, their contribution must be scaled accordingly. Introducing a scale weight that accounts for this volume ratio and assembling the RVE contributions gives the weighted micro-stiffness matrix $\tilde{\boldsymbol{K}}^{*}$ in Eq. (3). Let $\boldsymbol{P}$ denote the linear operator relating to the microscale and macroscale degrees of freedom:

$$\boldsymbol{u} = \boldsymbol{P}\tilde{\boldsymbol{u}} \tag{4}$$

The virtual work done by the macroscopic load $\boldsymbol{F}$ is then expressed in terms of microscale quantities, so that Eq. (3) can be recast as a single coupled system:

$$\widetilde{\boldsymbol{K}}^{*}\widetilde{\boldsymbol{u}} = \boldsymbol{P}^{\mathrm{T}}\boldsymbol{F} \tag{5}$$

2.1 Coupling of macro- and micro-elements

In this study, periodic boundary conditions (PBC) are applied for the linear coupling of the macroscale and microscale. Let $\widetilde{\boldsymbol{u}}$ denote the nodal displacement of the micro-element within the RVE, $\boldsymbol{u}$ the nodal displacement of the macro-element, and $\boldsymbol{\xi}$ the local coordinates. The nodal displacements of the RVE are related to the macroscopic displacement by

$$\widetilde{\boldsymbol{u}} = \sum N^{I}(\xi)\boldsymbol{u}^{I} \tag{6}$$

As shown in Fig. 1, the relative displacement constraint conditions between opposite boundaries (top-bottom, left-right) of the RVE are then defined as

$$\widetilde{\boldsymbol{u}}_{b} - \widetilde{\boldsymbol{u}}_{a} = \sum (N^{I}(\xi_{b}) - N^{I}(\xi_{a}))\boldsymbol{u}^{I} \tag{7}$$

$$\widetilde{\boldsymbol{u}}_{d} - \widetilde{\boldsymbol{u}}_{c} = \sum (N^{I}(\xi_{d}) - N^{I}(\xi_{c}))\boldsymbol{u}^{I} \tag{8}$$

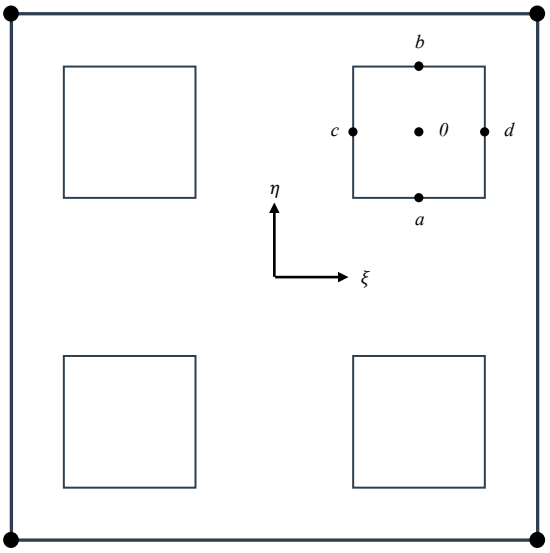

Fig. 1 4-node quadrilateral macro-element with RVEs located at the integration points under full integration.

To prevent rigid body motion and ensure convergence, an additional constraint condition is imposed on the center nodes of the RVE:

$$\widetilde{\boldsymbol{u}}_{0} = \sum N^{I}(\xi_{0})\boldsymbol{u}^{I} \tag{9}$$

2.2 Scale weighting

To compensate for the volume difference between the macro-element and the RVE, scale weights are derived from the principle of virtual work. The virtual work inside the macro-element and its approximation by Gaussian quadrature are given by

$$\delta W_{\mathrm{int}} = \sum_{e} \left(\int_{\Omega} \delta \boldsymbol{u}_{i,j} \boldsymbol{\sigma}_{ij} \mathrm{d}\Omega \right)_{e} \tag{10}$$

$$\delta W_{\text{int}} = \sum_e \left(\sum_G w_G J_G \left(\delta \boldsymbol{u}_{i,j}\right)_G \left(\boldsymbol{\sigma}_{ij}\right)_G \right)_e \tag{11}$$

Here, G is the integration point within the macro-element, w_G the corresponding integration weight, and J_G the Jacobian evaluated at that point. According to the Hill-Mandel condition, the macroscopic strains and stresses are defined as the volume average of the corresponding microscale fields over the RVE domain associated with the integration point:

$$\left(\delta \boldsymbol{u}_{i,j}\right)_G = \frac{1}{\Omega_G} \int_{\Omega_G} \delta \tilde{\boldsymbol{u}}_{i,j} \mathrm{d}\Omega \tag{12}$$

$$\left(\boldsymbol{\sigma}_{ij}\right)_G = \frac{1}{\Omega_G} \int_{\Omega_G} \tilde{\boldsymbol{\sigma}}_{ij} \mathrm{d}\Omega \tag{13}$$

Multiplying and rearranging these two equations yields

$$\frac{1}{\Omega_G} \int_{\Omega_G} \delta \tilde{\boldsymbol{u}}_{i,j} \mathrm{d}\Omega \cdot \frac{1}{\Omega_G} \int_{\Omega_G} \tilde{\boldsymbol{\sigma}}_{ij} \mathrm{d}\Omega = \frac{1}{\Omega_G} \int_{\Omega_G} \delta \tilde{\boldsymbol{u}}_{i,j} \tilde{\boldsymbol{\sigma}}_{ij} \mathrm{d}\Omega \tag{14}$$

Substituting Eq. (14) into the macroscale virtual work Eq. (11), the macroscopic virtual work is recast in terms of microscale quantities as

$$\delta W_{int} = \sum_e \left(\sum_G \frac{w_G J_G}{\Omega_G} \int_{\Omega_G} \delta \tilde{\boldsymbol{u}}_{i,j} \tilde{\boldsymbol{\sigma}}_{ij} \mathrm{d}\Omega \right)_e \tag{15}$$

The total internal virtual work of the microscale model is obtained by summing the contributions of the individual RVEs:

$$\delta \widetilde{W}_{int} = \sum_e \left(\sum_G \int_{\Omega_G} \delta \tilde{\boldsymbol{u}}_{i,j} \tilde{\boldsymbol{\sigma}}_{ij} \mathrm{d}\Omega \right)_e \tag{16}$$

Finally, enforcing the equivalence between Eqs. (15) and (16) at the integration points of a 4-node quadrilateral element yields the following scaling relation:

$$\frac{w_G J_G}{\Omega_G} = \frac{1}{4} \frac{V_e}{V_G} \tag{17}$$

Eq. (17) is implemented by scaling the geometric dimensions of the RVE so that the required volume ratio between the macroscale element and the RVE is recovered. The macro-nodes and RVE boundary nodes are linked through multi-point constraints (MPCs), and a negligible elastic modulus is assigned to the macro-element so that they contribute no stiffness while remaining available for visualization.

3. Homogenization method

In this study, the asymptotic expansion homogenization (AEH) method [12,13] is employed to predict the macroscopic behavior of composite materials. The core of AEH lies in a microscale RVE and an asymptotic expansion of the displacement field in the ratio of the microscale to macroscale lengths. The effective macroscopic properties derived through this are applied to the global structural analysis, which substantially reduces the computational cost while retaining the influence of the microstructural geometry on the macroscopic response.

In the AEH method, the displacement field is expanded asymptotically as

$$u_i^{\epsilon}(x) = u_i^{(0)}(x,y) + \epsilon u_i^{(1)}(x,y) + \epsilon^2 u_i^{(2)}(x,y) + \cdots \tag{18}$$

With the macroscale coordinate x and the microscale coordinate $y = x/\epsilon$, where $\varepsilon \ll 1$ is the ratio of the characteristic lengths of the two scales, the displacement field is approximated as the sum of macroscopic behavior and higher-order terms that carry microstructural information. The differential operator is decomposed into the sum of the macroscopic scale gradient and the micro-scale local gradient as

$$\frac{\partial}{\partial x_i^{\epsilon}} = \frac{\partial}{\partial x_i} + \frac{1}{\epsilon}\frac{\partial}{\partial y_i} \tag{19}$$

Applying Eq. (19) to Eq. (18), equilibrium equations in terms of the parameter ϵ can be obtained, and the first-order corrected displacement then holds the following relationship:

$$u_i^{(1)}(x,y) = -\chi_i^{kl}(y)\frac{\partial u_k^{(0)}}{\partial x_l} + \tilde{u}_i^{(1)}(x) \tag{20}$$

where $\chi_i^{kl}(y)$ are the components of the characteristic displacement tensor, and $\tilde{u}_i^{(1)}(x)$ is the integral constants, usually considered as zero. The characteristic displacement tensor is a key factor determining how the macroscopic strain $\frac{\partial u_k^{(0)}}{\partial x_l}$ is locally dispersed. Through asymptotic analysis, the characteristic displacement tensor $\boldsymbol{\chi}$ is the solution of the variational problem [13-16]:

$$\int_Y D_{ijkl}\frac{\partial \chi_k^{mn}}{\partial y_l}\frac{\partial v_i}{\partial y_j}\mathrm{d}y = \int_Y D_{ijmn}\frac{\partial v_i}{\partial y_j}\mathrm{d}y \quad \forall v_i \in V_y \tag{21}$$

where Y is the RVE domain, D_{ijkl} the components of the elastic modulus tensor, and V_y is the test function space satisfying periodic boundary conditions. Substituting the characteristic displacement tensor obtained from Eq. (21) gives the effective stiffness tensor D_{ijmn}^h, which serves as the constitutive basis for the macroscale structural analysis:

$$D_{ijmn}^h = \frac{1}{|Y|}\int_Y D_{ijkl}\left[\delta_{km}\delta_{ln} - \frac{\partial \chi_k^{mn}}{\partial y_l}\right]\mathrm{d}Y \tag{22}$$

4. Hybrid multiscale analysis method

By placing an RVE at each integration point of the macroscopic model of composite materials, the direct FE² method can consider path-dependent and localized nonlinear phenomena, such as damage and interfacial delamination [14]. As addressed previously, however, the computational cost increases rapidly with the number of integration points and iterations, which limits the applicability of the method to large structures. The homogenization technique, in contrast, considerably reduces the computational cost by representing the macroscopic behavior through effective properties, but it is inherently unable to capture complex nonlinearities within the microstructure. In this study, a hybrid framework that couples the direct FE² method with the homogenization method is developed for the efficient analysis of composite structures, considering interface damage within the RVEs. Fig. 2 illustrates the proposed hybrid method, in which direct FE² models are employed in the local regions containing interfacial damage, and a homogenized model is used in the remainder of the domain.

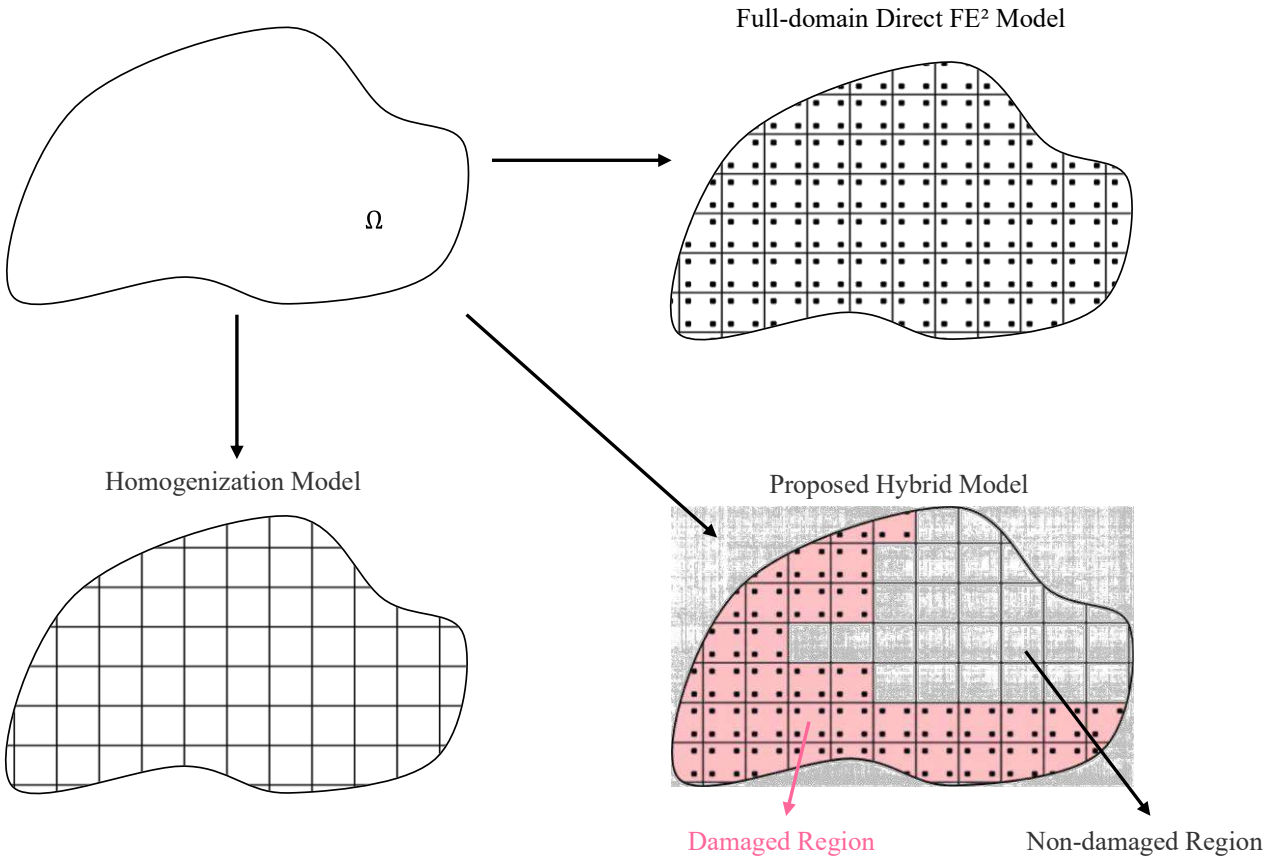

Fig. 2 Schematic of the present hybrid method coupling the direct FE^2 method with the homogenization method.

In this study, the homogenization method is first applied to the entire domain to obtain the macroscopic stress field. From this stress field, the regions requiring detailed analysis are identified, and direct FE² models are then placed to these regions. To identify the regions requiring detailed analysis, two criteria are introduced: the failure index (FI) and the stress gradient index (SGI). The FI is defined based on the Tsai-Wu failure criterion [15] to predict the regions where interface damage is likely to occur. These regions are replaced by fully-resolved RVEs with cohesive elements along the fiber-matrix interfaces, while the remainder of the domain is retained as homogenized elements. The FI is expressed as a quadratic function of stress components as

$$\mathrm{FI} = F_i^{(1)}\sigma_i + F_{ij}^{(2)}\sigma_i\sigma_j \tag{23}$$

where σ_i are the stress components in Voigt format, and $F_i^{(1)}$ and $F_{ij}^{(2)}$ are the strength parameters. Regions with $\mathrm{FI} < 1$ are regarded as undamaged, whereas interfacial delamination within the RVE is assumed to initiate once $\mathrm{FI} \geq 1$.

In the offline stage, the strength parameters of the FI are determined by analyzing an RVE under a set of training loads. In this study, three independent training loads of uniaxial tension, simple shear with the transverse displacement constraint, and bending are applied to a single two-dimensional RVE model with cohesive elements along the fiber–matrix interface. Additional training loads could be considered to further refine the strength parameters of the FI. As the training loads are increased, the damage behavior of the cohesive elements within the RVE is monitored to identify the onset of interfacial delamination. Specifically,

finite element analyses are performed for each of the three training loads, and the critical stress components at the onset of interfacial delamination are extracted. Substituting these stress components into Eq. (23) yields a system of simultaneous equations, from which the strength parameters $F_i^{(1)}$ and $F_{ij}^{(2)}$ are determined. When the number of these equations exceeds the number of unknown parameters, the strength parameters can be evaluated by least-squares regression, which minimizes the error across all sampled stress states. Since the Tsai-Wu failure criterion accounts for the combined effects of multi-axial stress states, the FI is expected to predict the initiation of interfacial delamination within RVEs under general stress states, and it therefore serves as the element replacement criterion in the hybrid algorithm. Fig. 3 shows the flowchart of the RVE training algorithm to determine the strength parameters of the FI.

The AEH method replaces a complex heterogeneous composite with an equivalent homogeneous macroscopic material. Since the homogenized model cannot represent local deformations within RVEs associated with a macro-element, its error grows as the stress gradient across the macro-element increases. The SGI is here defined as the variation in stress between the integration points of a macro-element. The stress variation of each element is normalized by the maximum von-Mises stress in the entire model, which suppresses the influence of low-stress regions. When the SGI of a macro-element exceeds a prescribed threshold, the homogenized elements are replaced by a direct FE^2 element, thereby reducing the error caused by high stress gradients within it. In this study, a threshold of 5% is adopted for the SGI criterion. This value is determined through a parametric study based on the error in the macroscopic reaction force, as detailed in Section 5.2. Fig. 4 illustrates the computational procedure for computing the SGI, which consists of evaluating the stress variations among the integration points of each macro-element, normalizing it by the maximum von-Mises stress, and applying the threshold-based switching criterion.

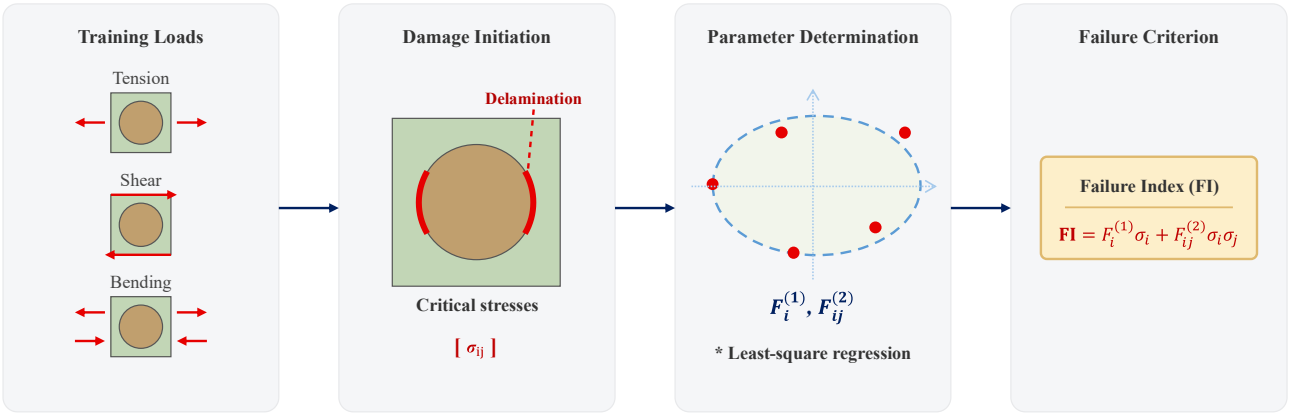

Fig. 3 Flowchart of the offline RVE training procedure for determining the Tsai-Wu-based failure index.

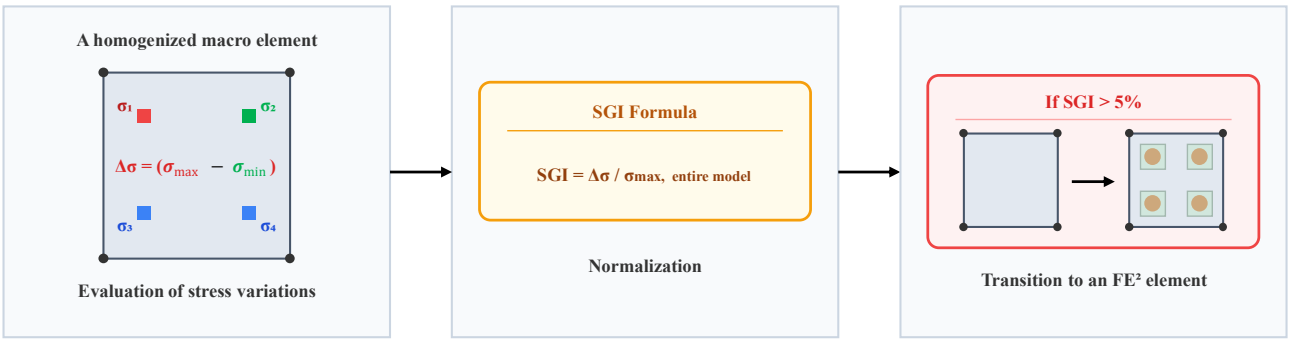

Fig. 4 Schematics of the computational procedure of the stress gradient index (SGI) and the associated element replacement.

The proposed algorithm automatically flags regions for detailed analysis when either the FI exceeds 1 or the SGI exceeds 5%. In the regions for detailed analysis, a direct FE² model is used to resolve interlayer delamination within RVEs and to capture high stress gradients in macro-elements, whereas homogenization elements are retained elsewhere to maintain computational efficiency. Fig. 5 presents the overall algorithm flowchart of the proposed hybrid multiscale analysis method.

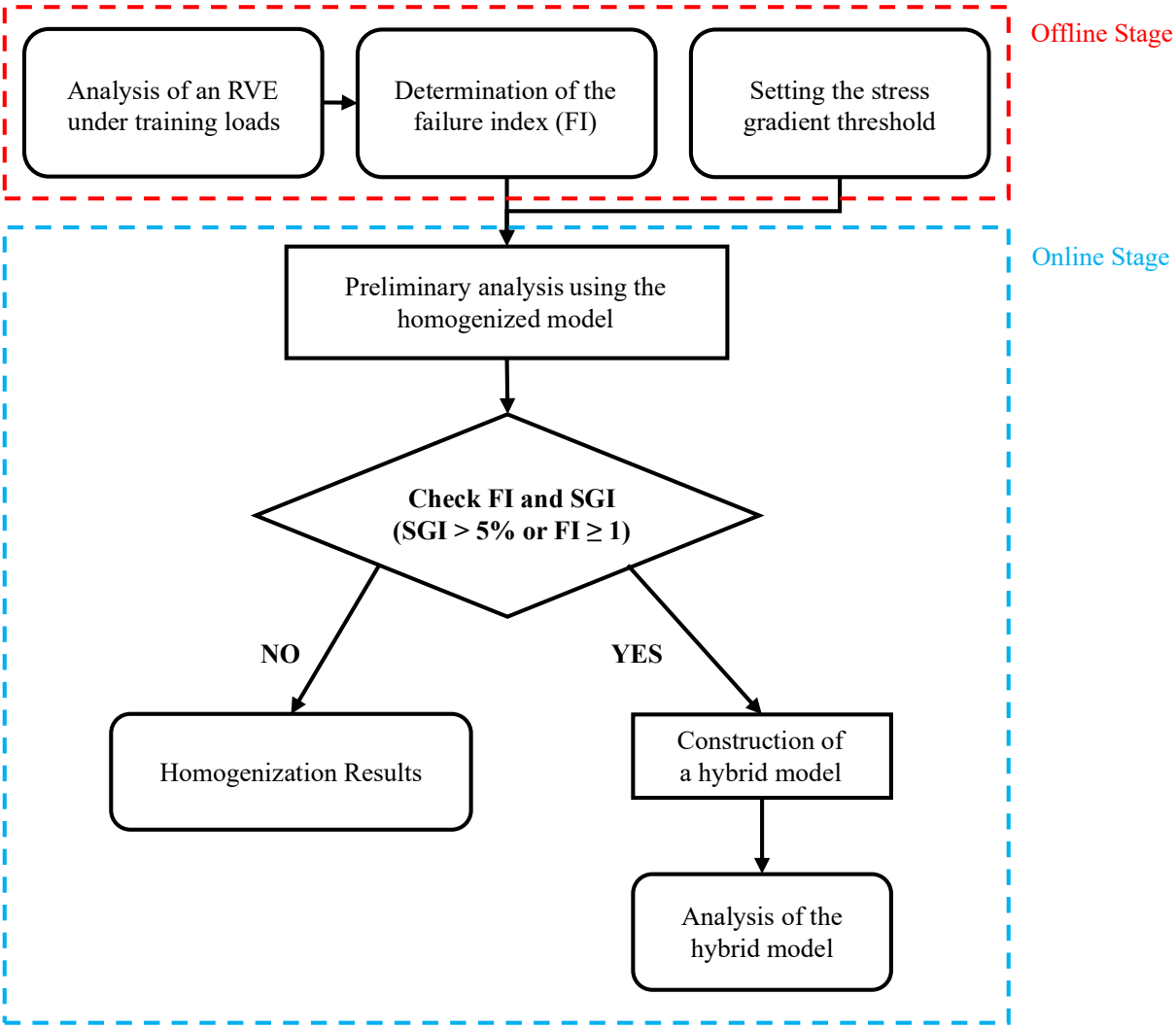

Fig. 5 Flowchart of the proposed hybrid direct FE² method for composite structures.

5. Numerical results

The accuracy and efficiency of the proposed hybrid multiscale method are demonstrated through several numerical examples. All analyses were performed using the commercial finite element analysis software Abaqus/Standard. In the FE^2 models, the fiber and matrix are discretized with 4-node plane stress elements (CPS4), and 4-node cohesive elements (COH2D4) are placed along the fiber–matrix interface to simulate interfacial delamination. As shown in Fig. 6, the RVE model consists of three components: the fiber, the matrix, and the cohesive interface. In all numerical examples, the size of the RVE is 10 mm, and the diameter of the fiber is 6 mm. To obtain the strength parameters of the FI for the hybrid algorithm, finite element analyses of the RVE model are performed under the training loads, as shown in Fig. 7.

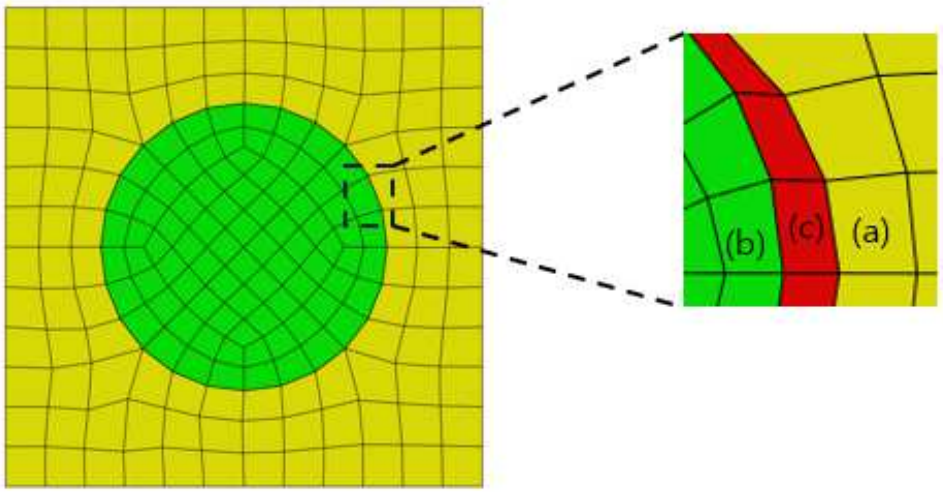

Fig. 6 Finite element model of an RVE: (a) matrix, (b) fiber, and (c) cohesive elements.

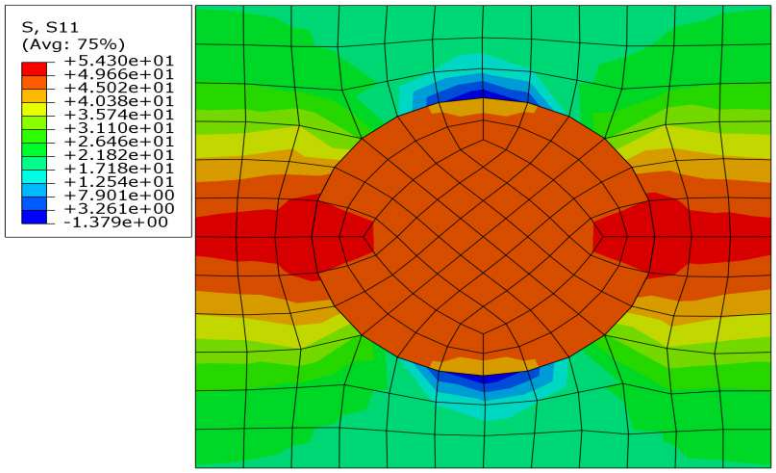

(a)

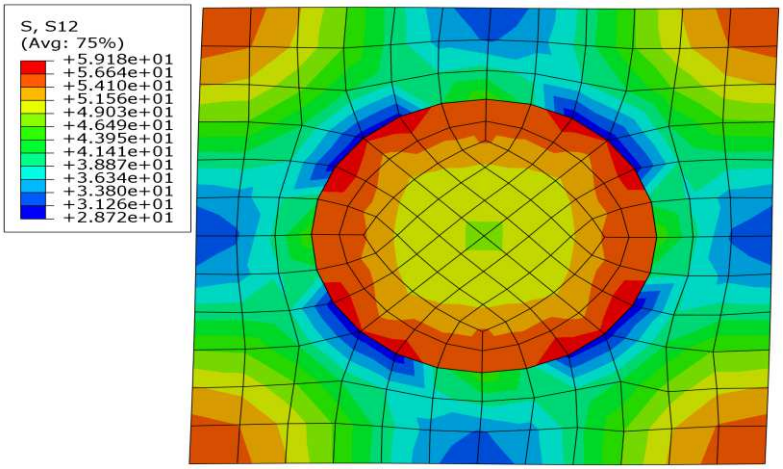

(b)

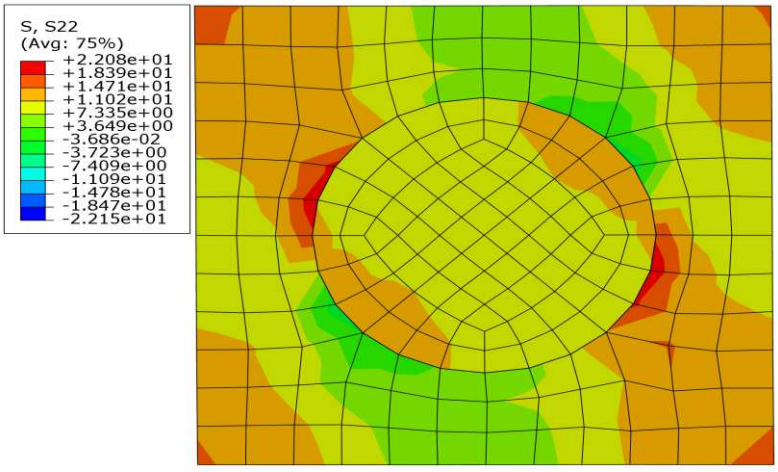

(c)

Fig. 7 Distributions of the von-Mises stress in the RVE model under the training loads used to determine the strength parameters of the failure criteria (FI): (a) uniaxial tension, (b) simple shear with the transverse displacement constraint, and (c) bending.

The material properties used for the RVE and the homogenized elements are listed in Tables 1-3. The effective elastic modulus of the RVE is given by

$$[\boldsymbol{D}_{\text{cohesive}}] = \begin{bmatrix} 6.1716 \times 10^3 & 1.8575 \times 10^3 & \approx 0 \\ 1.8575 \times 10^3 & 6.1712 \times 10^3 & \approx 0 \\ \approx 0 & \approx 0 & 1.8406 \times 10^3 \end{bmatrix} \quad (24)$$

The macro-stress field is first evaluated using the homogenized model, and the FI and the SGI are then computed to identify the regions requiring detailed analysis. These regions are then replaced by direct FE² domains, in which cohesive elements are placed along the fiber–matrix interfaces. In the Abaqus implementation, a Python script was utilized to dynamically replace the homogenized elements with detailed RVE domains based on the failure criteria, while enforcing nodal compatibility and displacement continuity along the boundaries between the homogenized and direct FE² regions. To establish the SGI threshold, which governs element replacement in the absence of damage, a preliminary analysis was conducted in the linear elastic regime, with the damage behavior of the cohesive elements temporarily deactivated. This procedure was implemented to rigorously isolate the errors arising purely from geometric stress concentrations from those induced by nonlinear material damage, thereby ensuring an objective and reliable threshold.

Table 1 Mechanical properties of composite materials

Material properties	Values
Young's modulus of matrix	$3.35GPa$
Poisson's ratio of matrix	0.35
Young's modulus of fiber	$230GPa$
Poisson's ratio of fiber	0.2

Table 2 Interfacial constitutive properties of cohesive elements

Material properties	Values
Normal stiffness	$1.0 \times 10^6 N/mm^3$
Shear stiffness	$1.0 \times 10^6 N/mm^3$
Normal strength	$1250MPa$
Shear strength	$1500MPa$
Mode I fracture energy	$400N/mm$
Mode II fracture energy	$1000N/mm$
BK power law exponent	1.45

Table 3 Mechanical properties of homogenized materials

Material properties	Values
Effective Young's modulus	$4.551GPa$
Effective Poisson's ratio	0.2313

Interfacial failure within the RVE is modeled by cohesive elements along the fiber-matrix interface, whose behavior is governed by a cohesive zone model (CZM) [16-18] relating to the crack opening displacement and the cohesive traction at the crack tip. A bilinear cohesive law [19], shown in Fig. 8, is adopted in this study. This law is defined by three parameters: the initial cohesive stiffness K_0, the cohesive strength σ_m, and the cohesive fracture energy G_C. Since composite interfaces are frequently subjected to mixed-mode stress states, the quadratic nominal stress criterion is used to determine damage initiation:

$$\left(\frac{\langle \sigma_{I} \rangle}{\sigma_{IC}}\right)^2 + \left(\frac{\sigma_{II}}{\sigma_{IIC}}\right)^2 + \left(\frac{\sigma_{III}}{\sigma_{IIIC}}\right)^2 = 1 \tag{25}$$

During damage propagation, the critical mixed-mode fracture energy is derived using the BK failure criterion [20,21] as

$$G^c = G_{IC} + \left(G_{IIC} - G_{IC}\right)\left\{\frac{G_{II} + G_{III}}{G_{I} + G_{II} + G_{III}}\right\}^{\eta} \tag{26}$$

In Eq (26), G_I, G_{II}, and G_{III} denote the cohesive energy in each mode, and η represents the material's intrinsic fracture exponent.

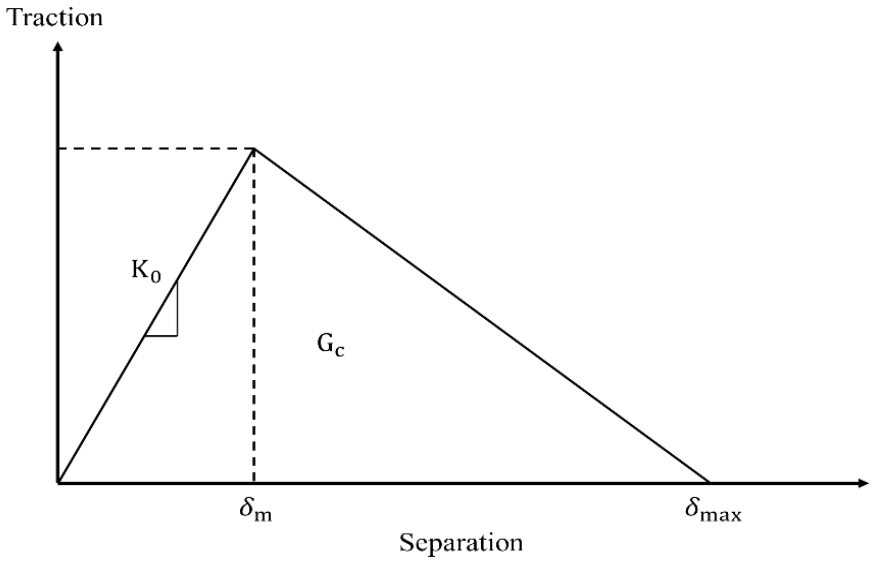

Fig. 8 Bilinear traction-separation law relating the cohesive traction to the crack opening displacement.

5.1 Hybrid analysis of a cantilever beam

As a first example, the proposed hybrid direct FE² method is applied to a cantilever beam. The dimensions of the beam are 200 mm × 80 mm, and the beam is discretized into 20×8 macro-elements. As shown in Fig. 9, a vertical displacement of 7 mm is applied downward at the right end of the beam, and the left end is constrained in the x-direction while lateral expansion is allowed to prevent artificial stress concentration caused by the Poisson effect. To quantitatively evaluate the accuracy and computational efficiency of the proposed hybrid direct FE² method, the results of the homogenization model and the hybrid model are compared with

those of the full-domain direct FE² model, which serves as the reference solution. The three analysis models are shown in Fig. 9.

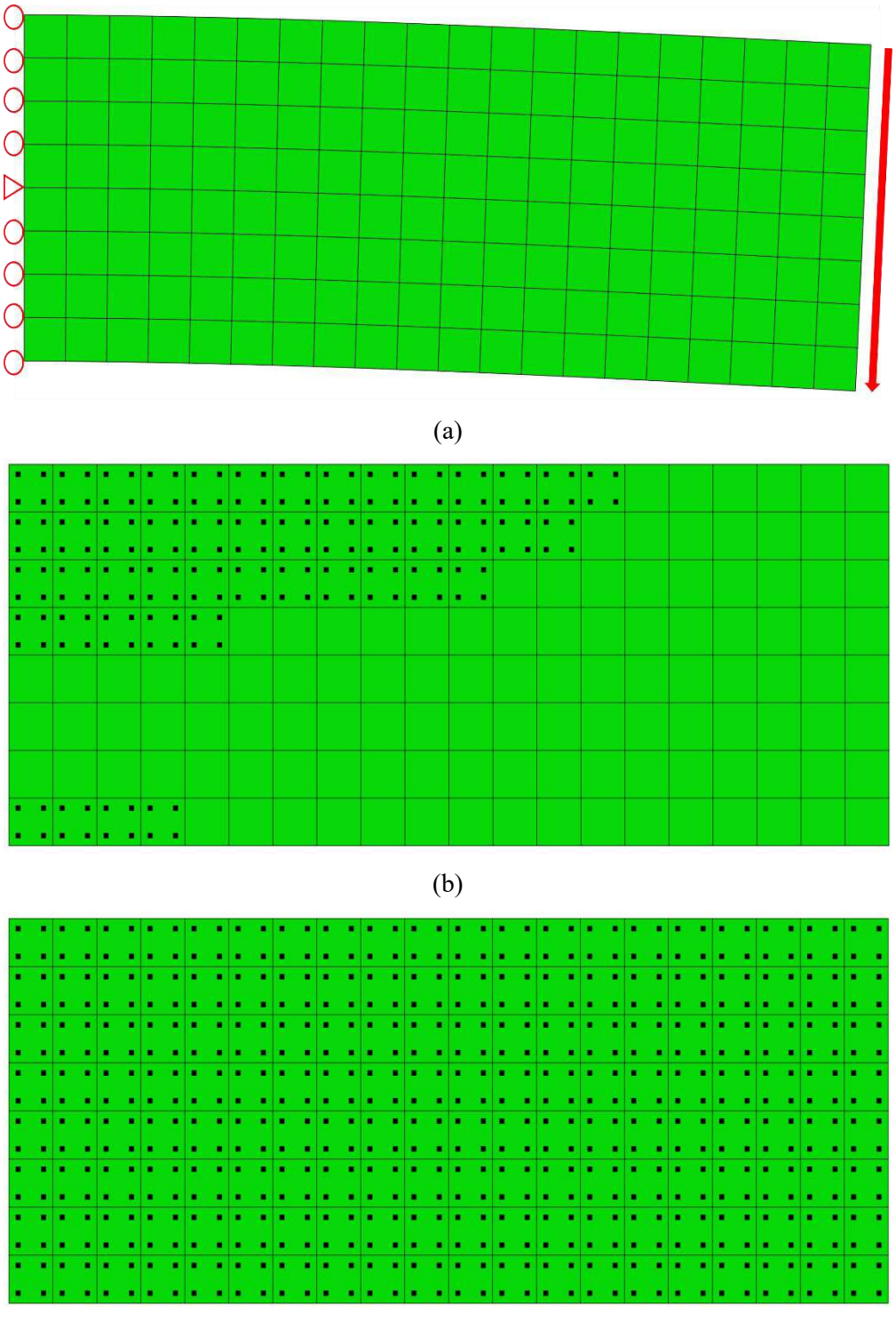

Fig. 9 Numerical models of the cantilever beam: (a) homogenized model, (b) hybrid model, and (c) full-domain direct FE² model.

The load-displacement curves of the cantilever beam obtained from the three analysis models are compared in Fig. 10. In the linear elastic regime, both the homogenization and hybrid models show excellent agreement with the reference solution. Once interfacial delamination initiates, however, the homogenization model fails to capture the nonlinear stiffness degradation. In contrast, the proposed hybrid model, which applies FE² elements only to the failure regions, closely follows the nonlinear response of the reference solution. The hybrid model predicts the final reaction force with an error of approximately 6.15%, whereas the homogenization model exhibits a larger error of approximately 23%. Furthermore, in terms of computational cost for the cantilever beam, the pure homogenization analysis required 15.2 s, and the full-domain detailed analysis 8410.2 s, whereas the proposed hybrid model completed the analysis in 2413.8 s. These results show that the hybrid direct FE² method successfully reduces the computation time by approximately 71.3% compared to the full detailed model while providing better agreement with the reference solution.

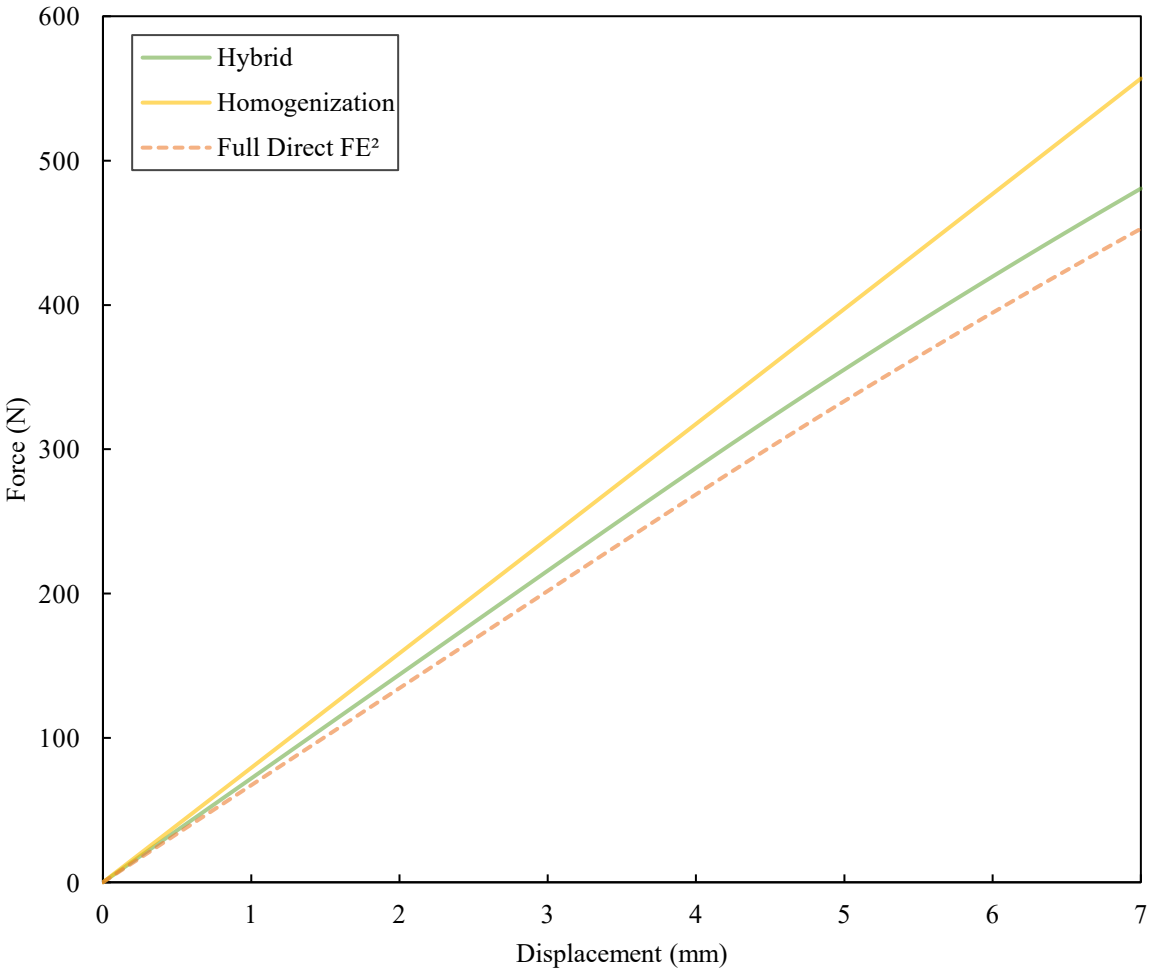

Fig. 10 Load-displacement responses of the cantilever beam obtained from the full-domain direct FE² model, the homogenization model, and the hybrid model.

5.2 Hybrid analysis of an S-shaped beam

As a second example, the proposed method is applied to an S-beam, whose geometric curvature induces a complex stress state. The dimensions of the S-shaped beam are shown in Fig. 11. Compared with the cantilever beam, this structure has a curved load transfer path and more widely distributed stress concentrations, making

it more critical to accurately capture local nonlinear fracture behavior and stress gradients. The boundary conditions are identical to those used for the cantilever beam: only the longitudinal (x-direction) displacements of the nodes at the left end are constrained so that artificial stress concentration caused by the Poisson's ratio effect is avoided. Although relying solely on the failure index (FI) is effective for relatively simple structures, it exhibits inherent limitations when applied to complex geometries such as the S-shaped beam. Because the single FI criterion alone cannot capture severe geometric stress concentrations prior to the onset of physical damage, it leads to errors in the predicted macroscopic stiffness. To overcome this limitation, the stress gradient index (SGI) is incorporated and combined with the FI to form a composite transition criterion. To determine an appropriate SGI threshold, a parametric study was conducted using the S-shaped beam benchmark. Four candidate thresholds (2.5%, 5%, 7.5%, and 10%) were evaluated by comparing the global reaction force response of the hybrid model against the full-domain direct FE² reference solution. Lower thresholds (e.g., 2.5%) resulted in unnecessarily broad regions to be replaced by the detailed RVE models, significantly reducing computational efficiency with only marginal gains in accuracy. Conversely, higher thresholds above 7.5% failed to capture sharp stress gradients, resulting in reaction force errors exceeding 10%. The 5% threshold provided the best balance between accuracy and efficiency, keeping the macroscopic error within an acceptable range while confining the detailed domain to critical regions only. Accordingly, a threshold of 5% was adopted for the SGI in the composite criterion. To demonstrate the advantages of the proposed technique, the results of the hybrid model based on the single FI criterion and that based on the composite (FI+SGI) criterion are compared with the full-domain direct FE² and homogenization solutions.

Fig. 11 compares the element replacement distributions of the two hybrid approaches for the S-shaped beam. Here, elements shown in red exceeded the transition criterion and are replaced with RVEs for direct FE² analysis, whereas those in gray remain macroscopic elements with homogenized properties. As shown in Fig. 11(b), when the FI criterion alone is applied, replacement is limited mainly to regions where physical failure was initiated. In contrast, the composite criterion proposed in this study (Fig. 11(c)) identifies regions of high stress gradient before physical damage occurs where the load path changes direction. As a result, the replacement region is allocated more extensively and in a more stable manner.

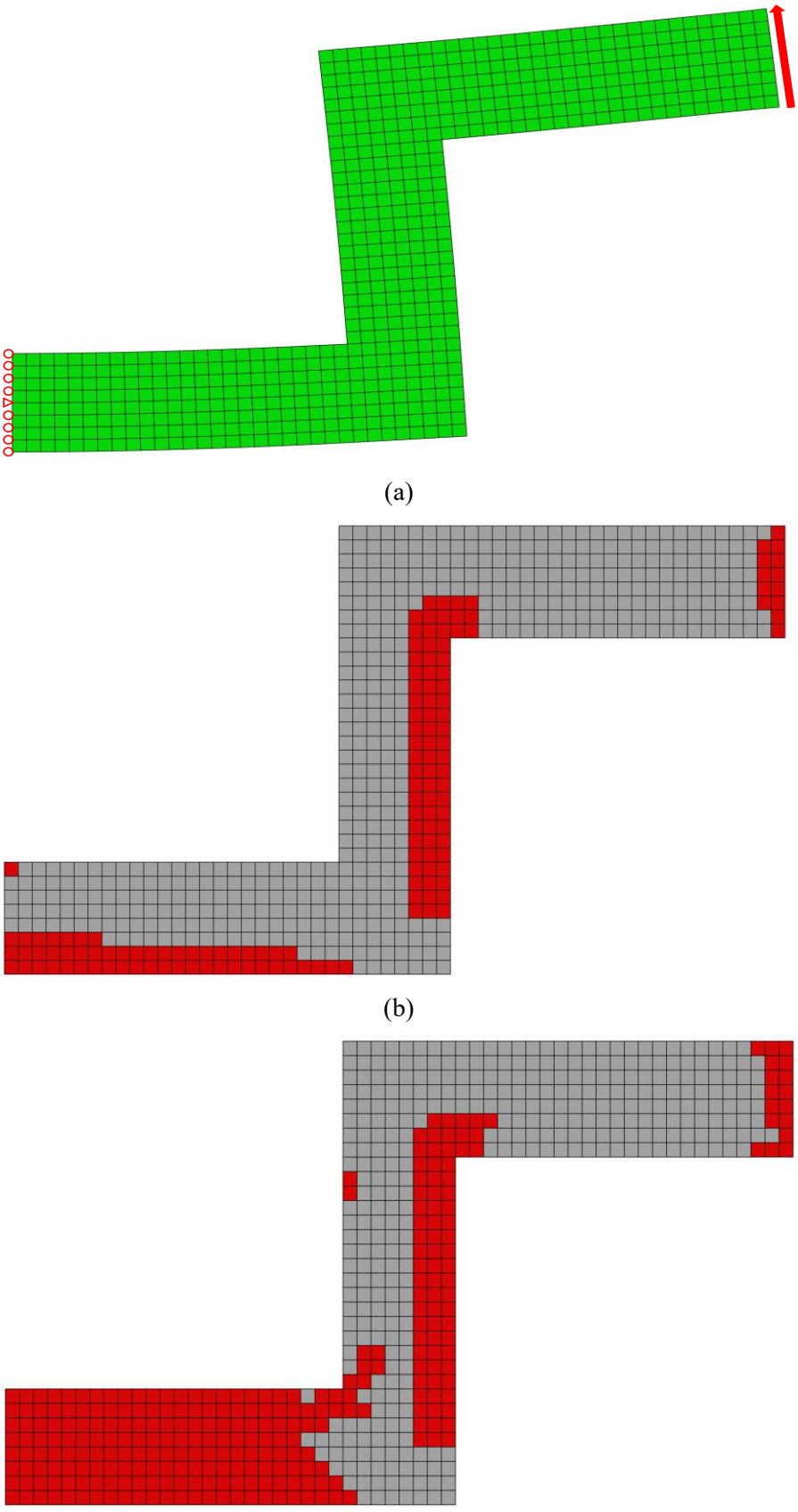

Fig. 11 S-shaped beam model: (a) geometry and boundary conditions; (b) element replacement distribution obtained with the FI criterion alone; (c) element replacement distribution obtained with the proposed composite FI + SGI criterion.

The effect of these different replacement strategies is clearly revealed in the load-displacement responses shown in Fig. 12. The pure homogenization method produces a reaction force error of about 35% and fails to reproduce the fracture behavior. The hybrid model with the FI criterion alone captures the final failure; however, because it does not detect the initial stress concentrations in the curved regions early enough, stiffness errors accumulate once the response becomes nonlinear. In contrast, the hybrid model with the proposed composite criterion replaces the initial stress concentration regions with RVEs before damage occurs, yielding a nonlinear response nearly identical to that of the full-domain direct FE² model. The final reaction force error is reduced to below 6%, demonstrating the high reliability of the proposed method. In terms of computational efficiency, although the composite criterion enlarges the replacement region, only 288 of the 640 macroscopic elements (approximately 45%) are replaced with direct FE² models. This indicates that the overall computational cost can be substantially reduced by selectively assigning RVEs only to local regions susceptible to stress concentration and damage. Overall, the S-shaped beam results indicate that the proposed hybrid direct FE² method is a versatile and practical framework, applicable even to structures with complex stress redistribution.

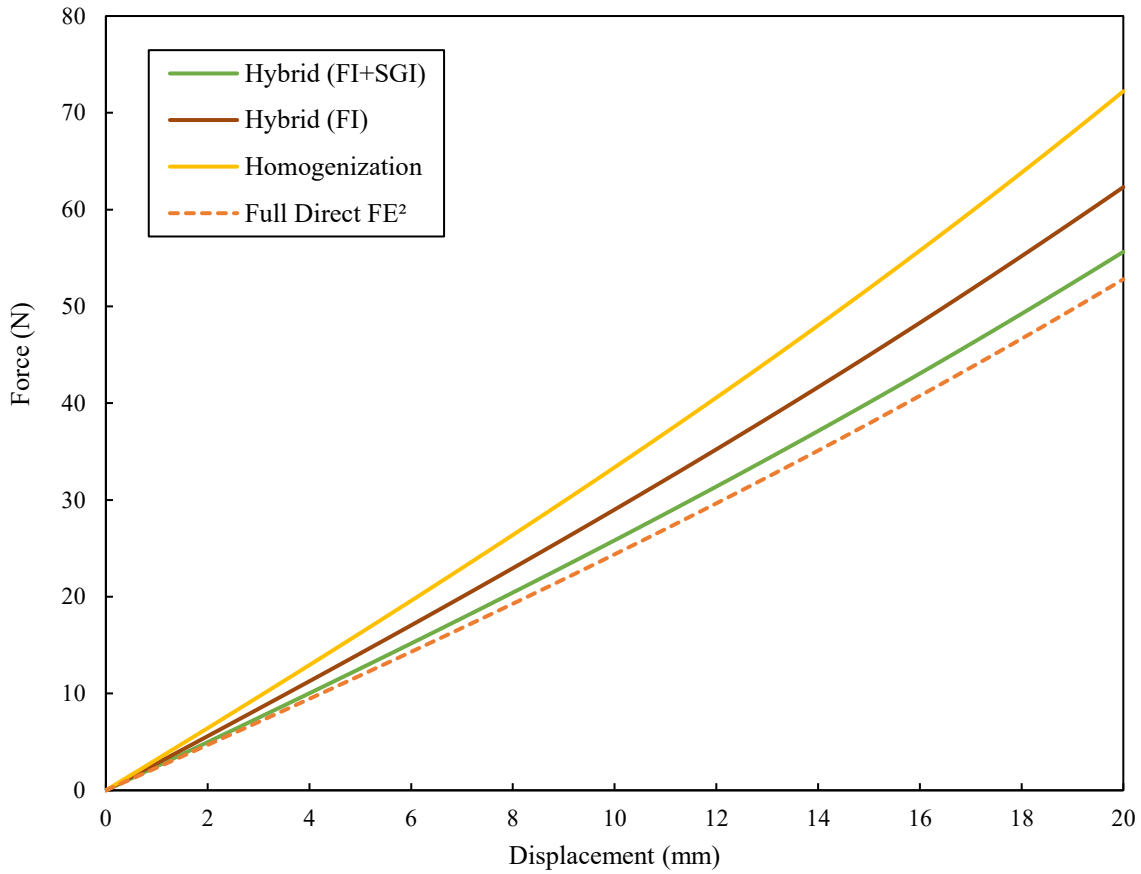

Fig. 12 Load-displacement responses of the S-shaped beam obtained from the full-domain direct FE² model, the homogenization model, the hybrid model with the FI criterion alone, and the hybrid model with the composite FI + SGI criterion.

5.3 Hybrid analysis of a mode I edge-cracked plate

As the final example, the proposed hybrid direct FE² method is applied to an edge-cracked composite plate under mode I loading to further verify its effectiveness. As shown in Fig. 13(a), a tensile load is applied to one end of the plate to induce singular stresses and delamination growth around the crack tip. Owing to the extremely steep stress gradients in this region, this example most clearly highlights the difference in performance between the single and composite criteria. Fig. 13 compares the element replacement distributions obtained with the single and composite criteria. When the FI criterion alone is applied (Fig. 13(b)), only a very few elements ahead of the crack tip, where failure is imminent, are replaced with RVEs for the direct FE² analysis. In contrast, the composite criterion (Fig. 13(c)) detects and replaces a broader region around the crack tip where the stress gradient changes sharply, even before physical failure initiates. Meanwhile, the homogenized model is retained in the outer region, where the stress field is relatively uniform.

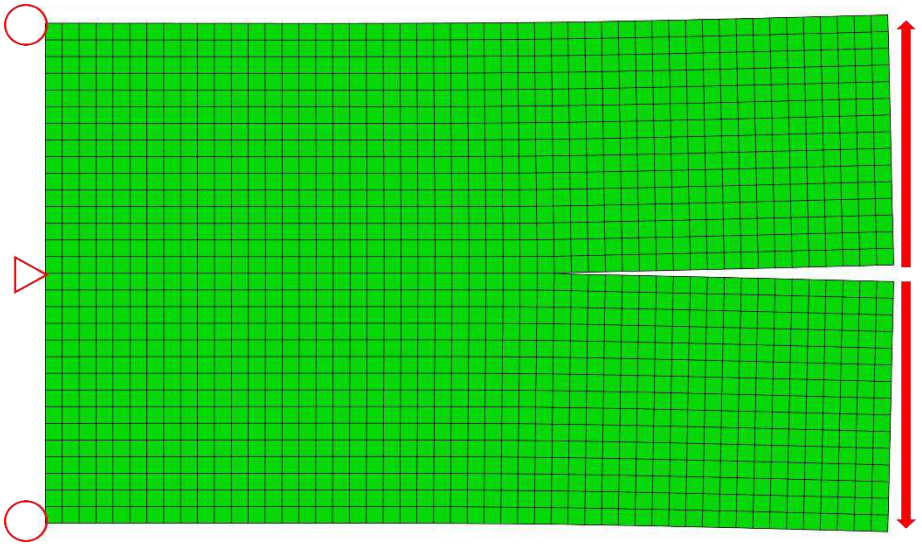

(a)

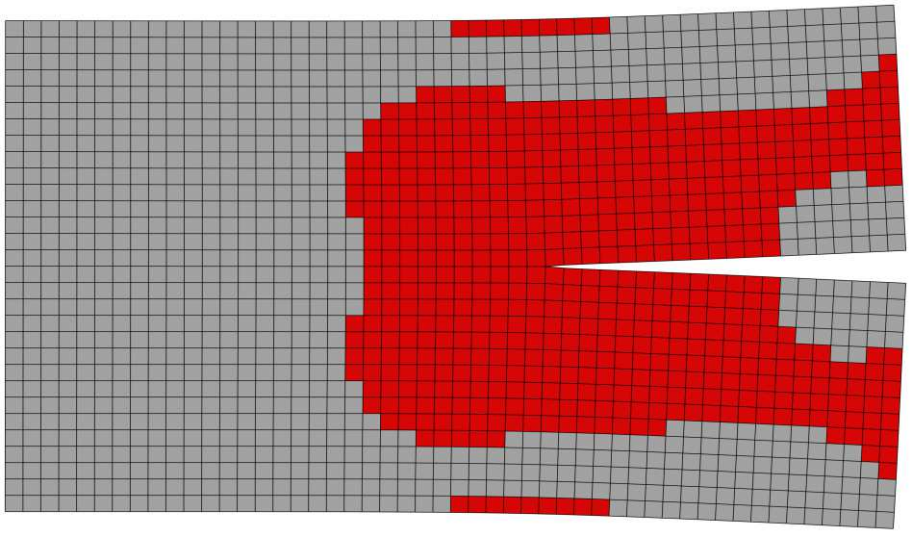

(b)

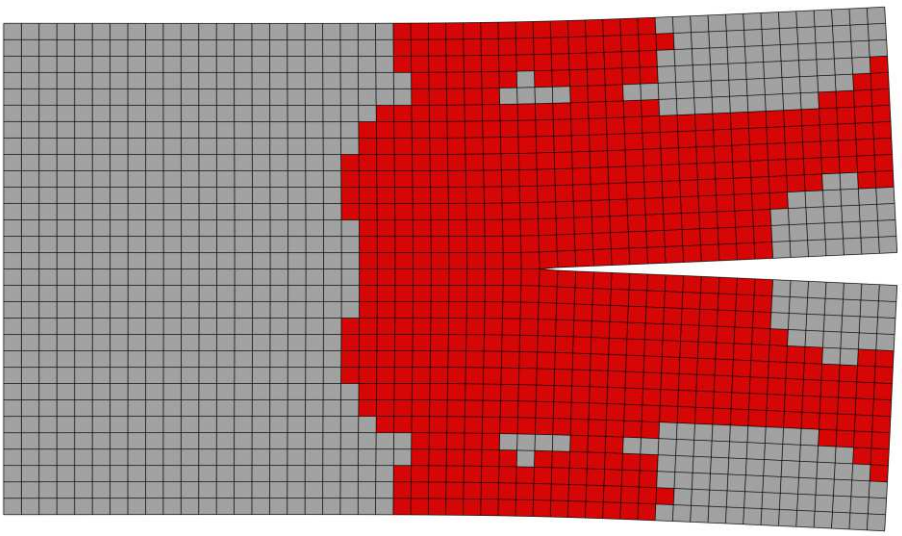

(c)

Fig. 13 Edge-cracked composite plate model: (a) geometry and boundary conditions; (b) element replacement distribution obtained with the FI criterion alone; (c) element replacement distribution obtained with the proposed composite FI + SGI criterion.

Fig. 14 clearly shows how these differences in replacement strategy affect the predicted load–displacement response. If regions with extreme macroscopic stress gradients, such as the crack tip, remain in the homogenization model, it leads to severe local stress errors due to the inherent limitations of first-order asymptotic homogenization. The FI-only hybrid model likewise fails to capture the initial stress gradient and therefore overestimates the stiffness at the onset of nonlinearity, deviating from the reference solution. In contrast, the composite-criteria hybrid model, which considers the stress gradient together, prevents such stress averaging errors and closely reproduces the nonlinear fracture behavior of the full-domain direct FE^2 model, with a reaction force error of 12.7%. In terms of computational efficiency, only 670 of the 1500 macroscopic elements (approximately 44.7%) are replaced with direct FE^2 models. These results indicate that selectively assigning RVEs only to the regions around the crack where damage is expected can substantially reduce the computational cost while maintaining acceptable accuracy. The results of the mode I edge-cracked plate demonstrate that the proposed hybrid direct FE^2 method remains effective even for problems involving strong discontinuities and steep stress gradients, such as cracks.

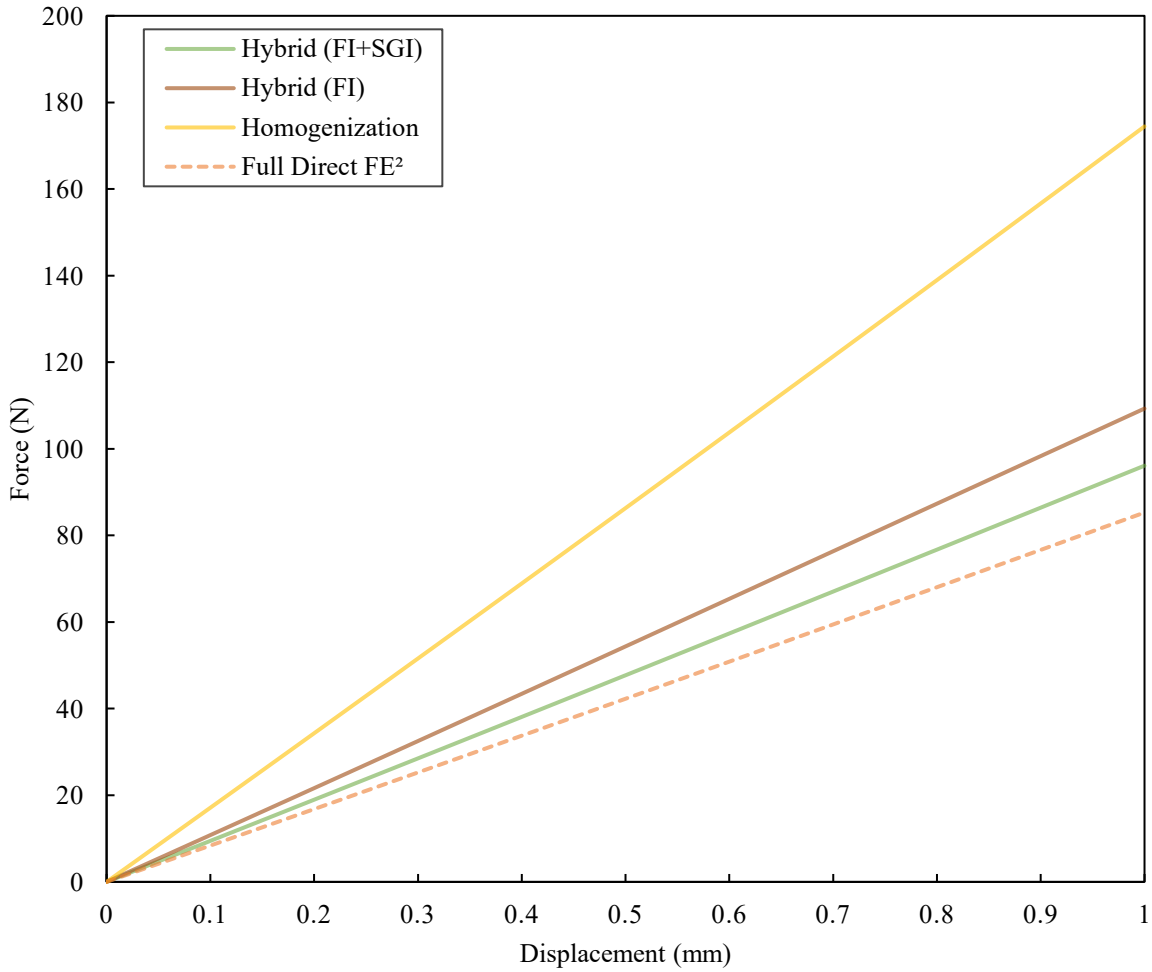

Fig. 14 Load-displacement responses of the mode I edge-cracked plate obtained from the full-domain direct FE^2 model, the homogenization model, the hybrid model with the FI criterion alone, and the hybrid model with the composite FI + SGI criterion.

5.4 Computational efficiency

To quantitatively assess the computational efficiency of the proposed hybrid direct FE^2 method, this section compares the computation times for the three numerical examples. Three approaches are compared: the full-domain direct FE^2 models, the homogenization models, and the hybrid models with the composite criterion. All analyses were performed in the same computing environment, and the computation times for the three approaches are summarized in Table 4. As shown in the results, the homogenization model requires the shortest computation time; however, as addressed earlier, it cannot capture local nonlinear fracture behavior. In contrast, the full-domain direct FE^2 model, which allocates RVEs to all integration points, provides the most accurate solution, but incurs a prohibitive computational cost, severely limiting its practicality for large-scale structures.

The proposed hybrid method selectively replaces RVEs only in local critical regions where failure was expected. Consequently, it requires somewhat more computation time than the homogenization model, but substantially less than the full-domain direct FE^2 model. Specifically, the hybrid model reduces the computation time by approximately 71.3% relative to the full-domain direct FE^2 model for the cantilever beam, and by 55.1% and 54.6% for the S-shaped beam and the edge-cracked plate, respectively. These reductions are

consistent with the element replacement ratios reported in Sections 5.2 and 5.3, indicating that the computational savings scale closely with the reduction in the size of the detailed analysis region. In conclusion, it is proven that the proposed hybrid direct FE² method substantially reduces the computational cost of multiscale analysis while accurately capturing both the global macroscopic response and the local interfacial delamination of the composite structures.

Table 4 Comparison of computation times for different multiscale analysis methods

Method \ Time (s)	Cantilever beam	S-shaped beam	Edge-cracked plate
Homogenization	15.2	39.7	85.1
Hybrid	2413.8	10951	25880
Full-domain direct FE²	8410.2	24371	56952

6. Conclusions

This study presents a hybrid analysis method that combines the high accuracy of the direct FE² method and the computational efficiency of the homogenization method. A composite criterion combining the Tsai–Wu failure index and the stress gradient index is introduced to automatically identify regions requiring detailed analysis and replace them with direct FE² elements. Since the remainder of the domain is represented by homogenized elements, the proposed method substantially reduces the computational cost while maintaining accuracy comparable to that of the full-domain direct FE² analysis. The proposed method is validated through three numerical examples: a cantilever beam, an S-shaped beam, and an edge-cracked plate. The numerical results demonstrate that the proposed method substantially improves the computational efficiency of simulating composite structures with microscale interfacial damage while maintaining accuracy. These findings are expected to facilitate more efficient progressive failure analysis of composite structures.

Acknowledgements

This research was supported by Basic Science Research Program through the National Research Foundation of Korea (NRF) funded by the Ministry of Education (No. 2022R1I1A2053461).

CRediT authorship contribution statement

Ju-Won Jin: Conceptualization, Methodology, Software, Validation, Formal analysis, Investigation, Writing - original draft, Visualization.

Hyun-Gyu Kim: Conceptualization, Methodology, Resources, Writing - review & editing, Supervision, Project administration, Funding acquisition.

Declaration of competing interest

The authors declare that they have no known competing financial interests or personal relationships that could have appeared to influence the work reported in this paper.

Data availability

All processed data required to reproduce these findings are presented in the article. The raw simulation files and automation scripts are available from the corresponding author upon reasonable request

References

1. Geers MGD, Kouznetsova VG, Brekelmans WAM (2010) Multi-scale computational homogenization: Trends and challenges. J Comput Appl Math 234:2175-2182.
2. Llorca J, González C, Molina-Aldareguía JM, Segurado J, Seltzer R, Sket F, Rodriguez M, Sádaba S, Muñoz R, Canal LP (2011) Multiscale modeling of composite materials: a roadmap towards virtual testing. Adv Mater 23(44):5130-5147.
3. Michel JC, Moulinec H, Suquet, P (1999) Effective properties of composite materials with periodic microstructure: a computational approach. Comput Meth Appl Mech Eng 172(1-4):109-143.
4. Feyel F, Chaboche JL (2000) FE² multiscale approach for modelling the elastoviscoplastic behaviour of long fibre SiC/Ti composite materials. Comput Meth Appl Mech Eng 183(3-4):309-330.
5. Kim KB, Kim HG (2025) Improvement of the Direct FE² method for multiscale analysis of composite materials. Multi Sci Eng 49(4):261-268.
6. Koliensnikova D, Ramière I, Lebon F (2020) Analytical comparison of two multiscale coupling methods for nonlinear solid mechanics. ASME J Appl Mech 87:094501-1.
7. Lloberas-Valls O, Rixen DJ, Simone A, Sluys LJ (2012) Multiscale domain decomposition analysis of quasi-brittle heterogeneous materials. Int J Numer Meth Eng 89(11):1337-1366.
8. Liu K, Meng L, Zhao A, Wang Z, Chen L, Li P (2023) A hybrid direct FE² method for modeling of multiscale materials and structures with strain localization. Comput Meth Appl Mech Eng 412:116080.
9. Gendre L, Allix O, Gosselet P, Comte F (2009) Non-intrusive and exact global/local techniques for structural problems with local plasticity. Comput Mech 44(2):233-245.
10. Belytschko T, Song JH (2010) Coarse graining of multiscale crack propagation. Int J Numer Meth Eng Vol. 81(5)537-563.
11. Hill R (1965) A self-consistent mechanics of composite materials. J Mech Phy Solids 13(4):213-222.
12. Kouznetsova V, Geers MGD, Brekelmans WAM (2002) Multi-scale constitutive modelling of heterogeneous materials with a gradient-enhanced computational homogenization scheme. Int J Numer Meth Eng 54(8):1235-1260.
13. Pinho-da-Cruz J, Oliveira JA, Teixeira-Dias F (2009) Asymptotic homogenization in linear elasticity. Part I: Mathematical formulation and finite element modelling. Comput Mater Sci 45:1073-1080.

14. Nguyen VP, Lloberas-Valls O, Stroeven M, Sluys LJ (2011) Computational homogenization for multiscale crack modeling. Implementational and computational aspects. Int J Numer Meth Eng 89(2):192-226.
15. Tsai SW, Wu EM (1971) A general theory of strength for anisotropic materials. J Composite Mater 5(1):58-80.
16. Park K, Paulino GH (2011) Cohesive zone models: a critical review of traction-separation relationships across fracture surfaces. Appl. Mech. Reviews 64(6):060802.
17. Choi YH, Kim HG (2020) Development of a cohesive zone model for fatigue crack growth. Multi Sci Eng 2(1):42-53.
18. Camacho GT, Ortiz M (1996) Computational modelling of impact damage in composite materials. Int J Solids Struct 33(20-22):2899–2938.
19. Turon A, Camanho PP, Costa J, Dávila CG (2006) A damage model for the simulation of delamination in advanced composites under variable-mode loading. Mech Mater 38(11):1072-1089.
20. Benzeggagh ML, Kenane M (1996) Measurement of mixed-mode delamination fracture toughness of unidirectional glass/epoxy composites with mixed-mode bending apparatus. Composites Sci Tech 56(4):439-449.
21. Camanho PP, Dávila CG, de Moura MF (2003) Numerical simulation of mixed-mode progressive delamination in composite materials. J Composite Mater 37(16):1415-1438.